Journal of Materials Chemistry A

ROYAL SOCIETY OF CHEMISTRY

PERSPECTIVE

View Article Online
View Journal | View Issue

Cite this: J. Mater. Chem. A, 2022, 10, 5889

Spatially resolved and quantitatively revealed charge transfer between single atoms and catalyst supports

Bin Di,† Zhantao Peng,† Zhongyi Wu, Xiong Zhou* and Kai Wu *

Received 27th September 2021
Accepted 3rd December 2021

DOI: 10.1039/d1ta08353h

rsc.li/materials-a

The charge state of supported single atoms is one of the most significant aspects determining the catalytic performance of single atom catalysts (SACs) which have drawn tremendous attention in recent years. In this perspective, mainly based on our previous studies and new data inputs, charge transfer between single atoms and their supports in several model systems is explored by the measurement of local work functions (LWFs). Two types of additives to tune the electronic properties of model catalysts, alkali metals and halogens, are described. The transferred charge is spatially resolved and quantitatively revealed based on LWF mapping *via* the Helmholtz equation. On average, Cs transfers more electrons than K does, echoing its lower first ionization energy. In contrast, Au and bromine atoms draw electrons from supports of metals like Cu and oxides like CuO. These insights into charge transfer at the atomic level are vital to understand their catalytic and promoting effects.

Introduction

Single atom catalysts (SACs), which essentially involve single-atom active sites on supports, have been extensively studied ever since the pioneering series of work by Zhang and co-workers in 2011.[1–11] Single atoms, which can be envisioned as being downsized from nanoparticles (NPs), may exhibit a superb catalytic performance in various catalytic reactions due to their low coordination number, strong metal–support interaction and quantized band structure or discrete energy levels. However, the inherent ineffectiveness for reactions that require simultaneous participation of more active metal atoms frequently prevents SACs from working, in addition to ever-changing interactions between the reactants and supported single atoms,[4,12–14] the available chemical environment and metal–support interactions.[15–18] The single active sites make SACs conceptually resemble a homogeneous catalyst, which enables the exploration of the catalytic mechanism by excluding the ensemble effect of supported NPs with a size distribution.[6] More importantly, the intrinsic properties of the single atoms are actually non-equal due to their non-uniform chemical environments on the support surfaces.[6]

One of the crucial factors discerning the catalytic activity is the charge state of the supported metal species that originates from charge transfer between the metal species and its support,[19] though a fierce debate on this has been going on. For example, both positively[2,3,20–23] and negatively[17,18,24,25] charged supported gold (Au) species are proposed to be responsible for the enhanced catalytic activity. Qiao *et al.*[1] reported that positively charged Pt single atoms were responsible for the excellent catalytic activity for CO oxidation while Therrien *et al.*[26] claimed that neutral Pt single atoms deposited on another support were also active. Therefore, a model system consisting of monodispersed single metal atoms on a well-defined oxide substrate serves as an ideal one where the charge state effect of an individual metal atom can be explored at the atomic level.

In contrast to extensively adopted approaches to anchoring single atoms, a new strategy to stabilize single atoms on supports is proposed in our previous study,[8] where the oxide support is made as thin as possible so that its surface free energy can be effectively augmented by its underlying bulk metal substrate. Once the surface free energy of the ultrathin oxide support becomes comparable with that of the metal species or chemical potential of an individual metal atom, the single metal atom can then be thermally stabilized on the ultrathin oxide film without aggregation. Based on this strategy, a thermally stable single-Au-atom model catalyst was successfully prepared by Zhou *et al.*[27] *via* thermal deposition of Au atoms onto a monolayered copper oxide (CuO) film grown on a Cu(110) substrate, and the Au single atoms did not aggregate up to 400 K. Therrien *et al.*[26,28] obtained stable single Pt atoms on a Cu_2O(111)-like single-layer film grown on the Cu(111) substrate and achieved low-temperature CO oxidation and water activation.

Apart from active metal atoms serving as catalytic centres in heterogeneous catalysts, additives are often introduced to further promote the performance of catalysts.[29–46] Among the additives, alkali metals[29–39] and halogens[40–46] are two types of

BNLMS, College of Chemistry and Molecular Engineering, Peking University, Beijing 100871, China. E-mail: kaiwu@pku.edu.cn; xiongzhou@pku.edu.cn

† These authors contributed equally.

promoters that are employed to tune the electronic properties of supported catalysts due to their capabilities[47–49] of electron donation and acceptance, respectively. As such, both promoters can induce an intense interfacial charge transfer that greatly changes the electronic properties of the metal species and support in the heterogeneous catalyst.

In the past, conventional surface techniques providing statistical and averaged information have been applied to study alkali metals and halogens on various substrates.[50–65] It's generally recognized that alkali metals and halogens on metal substrates result in the decrease and increase of the work functions (WFs) of metal substrates, respectively.[50,55,58–67] The same scenario also holds true on oxide surfaces where the introduced alkali metals often invoke more localized charge transfer.[68,69] However, such a picture for the charge transfer between these two types of promoters and their supports remains actually vague and ambiguous at the atomic level. Therefore, quantitatively unravelling the functionalizing range and extent of the impact by the charge transfer is of great significance to clarify the promoter effect of alkali metals and halogens. In our group, Peng *et al.*[70] recently showed that potassium cations (K^+) were spontaneously formed on a monolayered CuO film grown on Cu(110), leading to the decrease of the local WF (LWF) around each K^+ cation, while Chen *et al.*[71] observed that K atoms deposited on a monolayered ceria island grown on Pt(111) induced a significant decrease of the apparent LWF over the whole island.

The LWFs can be measured by scanning probe microscopy techniques with an extremely high spatial resolution, including scanning tunnelling microscopy (STM) and Kelvin probe force microscopy.[72–85] These techniques have been extensively applied to acquire the information of charge transfer[82–84] or redistribution.[73,74,85] Moreover, the surface dipole change[86–88] could be precisely extracted from the LWF variation ($\Delta\phi$). The methodology based on tunnelling current *versus* tip–sample distance (I–z) curves acquired by STM to deduce the LWF has been well established. Albrecht *et al.*[89] have elucidated that it is not suitable to determine $\Delta\phi$ on the atomic length scale *via* I–z spectroscopy, while Huang *et al.*[81] have demonstrated that it is bias voltage dependent upon the LWF measurements of thin oxide films on metal substrates, and LWF mappings with high spatial resolution can be accurately obtained at bias voltages close to zero. In principle, the apparent barrier height (ϕ_a), also known as apparent WF which is approximately equal to an average WF of the tip (ϕ_t) and the sample (ϕ_s), can be quantitatively obtained by recording the tunnelling current as a function of the tip height. It can be expressed by the following equations,[79,90–92]

$$\phi_a = 0.925 \times (\mathrm{d}\ln I/\mathrm{d}\ln z)^2$$

$$\phi_a = (\phi_t + \phi_s)/2$$

where I, z and ϕ are correspondingly in the units of ampere, angstrom, and electron volt.

Under the same tip conditions, the $\Delta\phi$ between two sampling spots, denoted as A and B, on the surface can be derived as,

$$\Delta\phi = \phi_s(\mathrm{B}) - \phi_s(\mathrm{A}) = 2 \times [\phi_a(\mathrm{B}) - \phi_a(\mathrm{A})]$$

Treating the single atoms as the adsorbates, the Helmholtz equation[93] can be used to describe the variation of the work function:

$$\Delta\phi = \mu\sigma/\varepsilon_0$$

where μ is the dipole moment that originated from the adsorbates ($\mu = ql$, q is the transferred charge and l is the distance between the charge centres); σ represents the adsorbate density and ε_0 is the dielectric constant. Thus

$$\Delta\phi = ql\sigma/\varepsilon_0 = \rho l/\varepsilon_0$$

where ρ is the charge density. Based on the single atom model, the quantity of the transferred charge can be calculated by the integration of the LWF change *via* the area influenced by the single atom:

$$\mathrm{Q} = \int \rho \mathrm{d}S = \int \Delta\phi \mathrm{d}S/l\varepsilon_0$$

l can be estimated from the height of the single atom.

In the past few decades, plenty of SACs have been prepared and reported.[2,6–8,94–111] However, the insight at the atomic level of charge transfer between single atoms and their supports is still elusive. A clear picture of charge transfer can obviously help understand the extraordinary catalytic performance of SACs as well as the promoter effects of alkali metals and halogens in conventional heterogeneous catalysis.

In this perspective, we summarize some of our recent studies on and new data inputs of charge transfer by means of apparent LWF mapping or $\Delta\phi$ mapping, and present an atomic view of the interaction between single atoms and substrates, demonstrating the availability and powerfulness of such a methodology. As mentioned above, three typical model systems will be described herein, namely, oxide-supported single Au atoms, oxide-supported alkali metal atoms and metal-supported halogen atoms.

Oxide-supported single Au atoms

By application of the strategy proposed by our group to mediate the surface free energy, a stable Au single-atom model catalyst on a monolayered CuO film grown on Cu(110) has been successfully prepared.[27] The CuO monolayer with a unit cell of 0.36 nm × 0.51 nm, being 1 × 2 times those for the pristine Cu(110) surface, which has been well confirmed,[112–116] was prepared by the exposure of the Cu(110) substrate to O_2 at room temperature (RT) and subsequent annealing at 500 K. The white protrusions in the STM image of the CuO monolayer with an atomic resolution represent the Cu cations, as shown in Fig. 1a. At RT, Au atoms are deposited on the CuO monolayer and exist as single atoms (yellow protrusions in Fig. 1a). High-resolution STM imaging (inset in Fig. 1a) reveals that the Au single atom is located at the hollow site of four Cu cations, *i.e.*, the bridge site of two O anions along the [1$\bar{1}$0] direction where the Au single

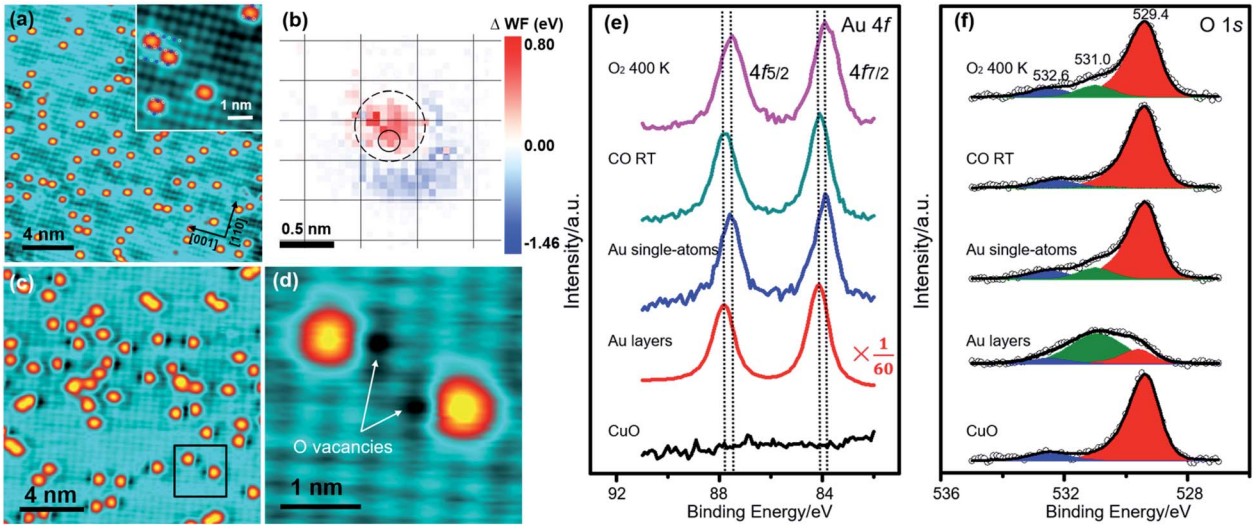

Fig. 1 Au single atoms on the CuO monolayer before and after the reaction with CO. (a) STM image of the Au single atoms on the CuO monolayer obtained by the deposition of 0.05 ML Au at RT. Inset: enlarged STM image of the Au single atoms. (b) $\Delta\phi$ mapping of an individual Au atom on the CuO monolayer. The black circle indicates the location of the Au single atom and the grey grid represents the lattice of the Cu cations. (c) STM image of the Au single atoms exposed to 18 L CO at RT. (d) Enlarged STM image of the square area marked in panel d. XPS spectra of the (e) Au 4f and (f) O 1s peaks of different samples. Red: normal O anions in the CuO monolayer; green: O anions in the CuO monolayer that interact with the Au atoms; blue: chemisorbed O species. Reproduced with permission (a and c–f).[27] Copyright 2018, American Chemical Society.

atom is stabilized by the Au–O interaction, as confirmed by the X-ray photoelectron spectroscopy (XPS) spectra of O 1s peaks at 531.0 eV in Fig. 1f. This Au single-atom model catalyst remains unchanged up to 400 K.

The $\Delta\phi$ mapping of the Au single atoms on the CuO monolayer is shown in Fig. 1b. An obvious increase of the LWF appears at the Au single atom site and its neighbouring area within about 0.5 nm around the Au atom, which implies the superposition of the intrinsic surface dipole by an induced dipole pointing to the vacuum. The LWF increase means negative charging of the Au single atom, which is also evidenced by the downshifted binding energy (BE) of the Au single atom with respect to a very thick neutral Au film, as shown in Fig. 1e. Therefore, the LWF increase is a consequence of electron transfer from the CuO substrate to the Au single atom. Consequently, a positively charged zone on the CuO substrate is created underneath the formed Au atom. It should be pointed out that the maximum value of $\Delta\phi$ does not appear precisely at the location of the Au atom. Such a local charge transfer could alter the electronic properties of the underlying CuO support around the Au atom.

The negatively charged Au atoms are active for CO oxidation. Fig. 1c shows the STM image of the Au SAC upon its exposure to CO at RT where dark features routinely appear nearest to the Au single atoms. High-resolution STM imaging (Fig. 1d) reveals that the dark features are precisely located at the positions of the O anions nearest to the single Au atoms and hence ascribed to lattice O vacancies in the CuO monolayer which are generated by CO oxidation with adjacent lattice O anions. This is also proved by the BE change of the O 1s peak at 531.0 eV. It's noticeable that once one of the two equivalent O anions nearest to the single Au atom is depleted upon CO oxidation, the negatively charged Au atom becomes electronically neutralized and hence inactive for further CO oxidation. Such changes in the charging state of the Au atom and its reaction activity towards the CO oxidation are also confirmed by the XPS data as shown in Fig. 1e and f. However, the activity of the Au atom can be restored by fixing the O vacancies with incoming oxygen molecules at higher temperatures, which again supports that the negatively charged Au atom is active for the CO oxidation.

Obviously, the charge transfer from the monolayered CuO support to the Au single atoms plays a key role in the CO oxidation where the negatively charged Au atoms are active and their neutralized counterparts are inactive. However, the apparent charge transfer extent, *i.e.* the number of electrons transferred onto each Au atom from the CuO substrate, and the influencing regime of the negatively charged Au atom on the CuO substrate cannot be quantitatively disclosed by conventional surface techniques like XPS. According to $\Delta\phi$ mapping, the transferred charge can be calculated as $Q = \int\Delta\phi \mathrm{d}S/l\varepsilon_0$. In addition, it's frequently noticed that the charge transfer of single atoms locally takes place around each atom within a small area. For instance, the single Au atom transfers the charge within an area of about 0.5 nm in diameter. Therefore, $\int\Delta\phi \mathrm{d}S$ is simply estimated as average $\overline{\Delta\phi}$ times the influenced area. Here, $\overline{\Delta\phi} = 0.6$ eV; $S = \pi d^2/4$; l is the height of the single Au atom, about 0.2 nm. Consequently, the transferred charge onto each Au atom is about $0.03e$. This quantitatively reveals how intensely the Au single atom electronically interacts with its underlying CuO substrate. It also helps rationalize the experimental observation that the incoming CO can only deplete the lattice O nearest to the negatively charged Au atom, leading to

the loss of its activity towards CO oxidation upon generation of one O vacancy nearest to it. Therefore, the high-resolution LWF mapping of a modelled SAC turns out to be very powerful and can provide quantitatively revealed and spatially resolved information to help understand the catalytic performance of SACs at the sub-nanometric level.

Oxide-supported single alkali metal atoms

Using the same monolayered CuO film grown on Cu(110), one can also explore the charge transfer between an individual alkali metal atom and its support, as recently reported by Peng *et al.*[70] from our group.

Thermally deposited K atoms at low coverage on the CuO monolayer are spontaneously ionized at RT and become positively charged. The K cations (termed K_A) are monodispersed, as shown in Fig. 2a. Its atomically resolved STM image in Fig. 2b demonstrates that K_A is located on the right top of a Cu cation or at the bridge site of two O anions along the [001] direction. Unlike the situation on the hydroxylated TiO_2(110) surface where the K atoms can be manipulated by the STM tip to preferentially move along the [001] direction,[117] the K_A cations on the CuO monolayer are extremely immobile. As K_A is positively charged, it is anticipated that the LWF around K_A will decrease due to the formation of an opposite surface dipole pointing from the K cation to the induced image charge underneath the surface. The $\Delta\phi$ mapping around K_A in Fig. 2c indeed shows a conspicuous LWF decrease within about 1.0 nm around K_A, in agreement with the XPS-measured BE of the K 2p feature (Fig. 2g) that a lower BE shift is observed for the sample with single K atoms (0.5 ML) with respect to the reference sample with high coverage (4 ML) K. Similarly, the transferred charge can be estimated by LWF mapping to be about 0.22|*e*| per K atom. Compared to the Au anion, both the influencing area and transferred charge of K_A are larger than those of the Au single atom.

Upon applying a sudden voltage pulse of +6 V on the K_A cation, the protrusion turns into a rectangular depression (termed K_B) which is randomly located at one of the four hollow sites surrounded by four Cu^{2+} cations nearest to the manipulated K_A, as shown in Fig. 2d and e. This tip manipulation process is reversible by switching the polarity of the pulsed voltage, *i.e.*, from +6.0 V to −6.5 V, the K_B species switches back to K_A again, but the restored K_A may jump back on top of either of the four equivalent Cu^{2+} cations nearest to K_B. Because of no obvious influence on the LWF of the CuO substrate around the K_B species, it is deducted that K_B is actually a neutral K atom, as shown in Fig. 2f.

Cesium (Cs) is bigger in size and lower in first ionization energy than K. Similarly, Cs atoms are also monodispersed on the monolayered CuO substrate upon their thermal deposition at RT. However, the monodispersed Cs atoms may sit on two different sites, either on top of the Cu cation, termed Cs_T, or at the hollow site surrounded by four Cu cations, termed Cs_H, as shown in Fig. 3a and b, respectively. To figure out the charge transfer between these two Cs species and the underlying CuO substrate, the apparent LWFs are measured and the $\Delta\phi$ mappings around Cs_T and Cs_H are depicted in Fig. 3d and e, respectively. With reference to its corresponding STM image, it is clear that the apparent LWF on the Cu–O chains becomes higher than that between two Cu–O chains and the maxima of the apparent LWFs spatially appear on the Cu cations. This is counterintuitive because cations generally induce a decrease in

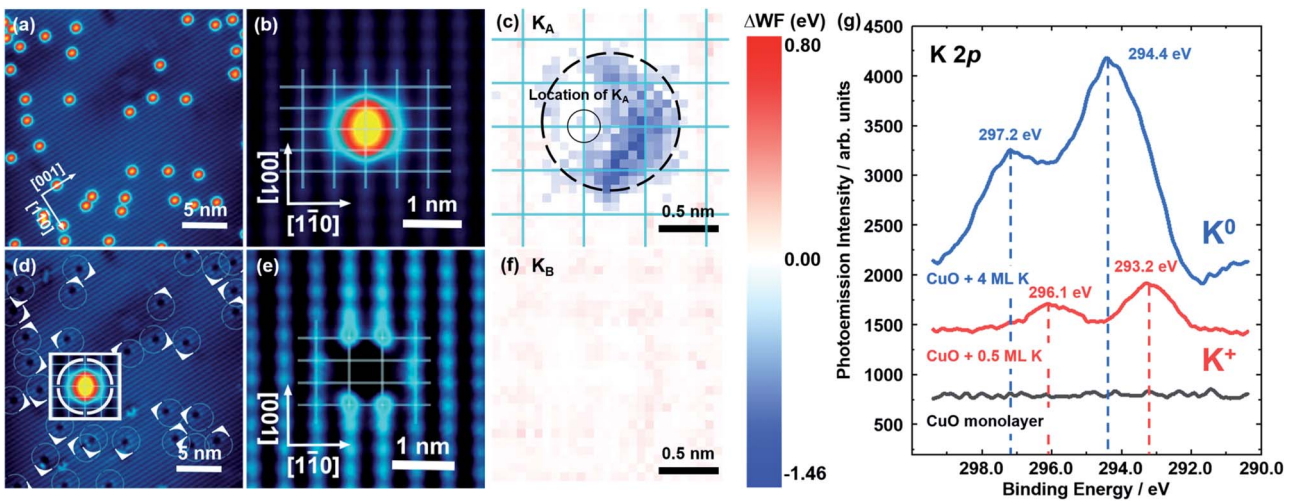

Fig. 2 (a) Large-scale STM image of monodispersed K cations (about 0.1 ML). (b) High-resolution STM image of a K cation supported on an ultrathin CuO film, termed K_A. (c) $\Delta\phi$ mapping of K_A. The cyan grid schematically represents the periodical Cu^{2+} lattice arrangement. (d) After high bias pulse treatments of all K cations in (a), most K_A cations switch into K_B. (e) High-resolution STM image of K_B. Inset: the quartering-encircled K_A highlights four possible jumping directions of the K species during the switching processes. The corresponding jumping direction for each K_B is also highlighted by the straight arrowheads in (d). (f) $\Delta\phi$ mapping of K_B. (g) XPS measurements of the pristine ultrathin CuO film (black curve), 0.5 ML K (red curve), and 4.0 ML K (blue curve) deposited onto the ultrathin CuO film. Reproduced with permission.[70] Copyright 2020, Wiley-VCH.

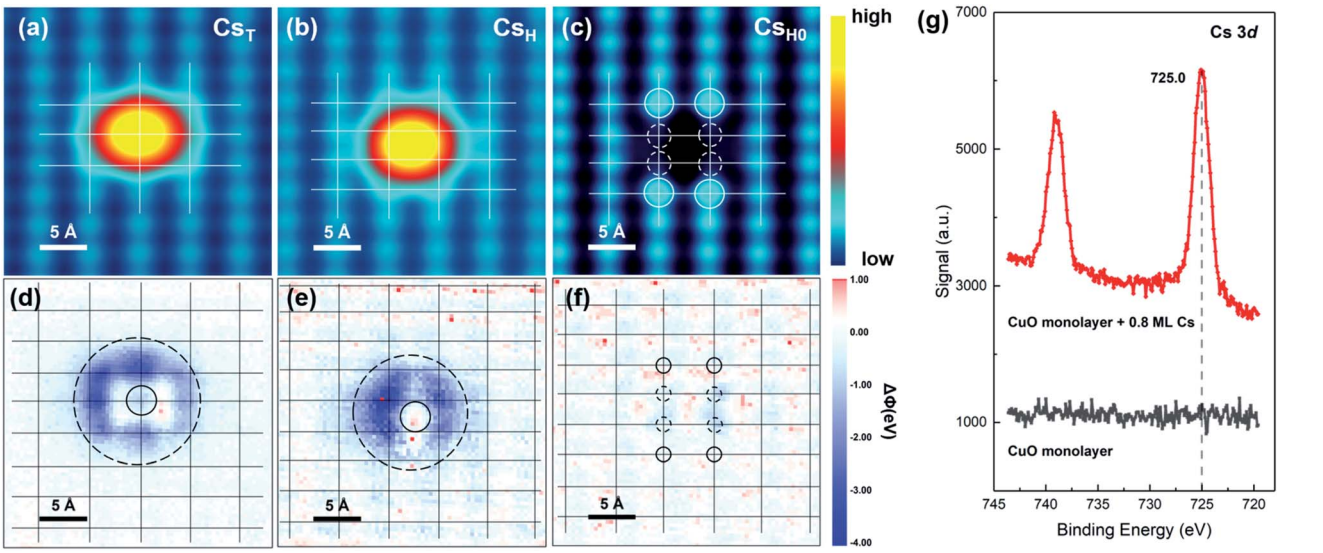

Fig. 3 High-resolution STM images of the Cs cations located on the (a) top and (b) hollow sites of the Cu cations, termed Cs_T and Cs_H, respectively. (c) Application of a +5.0 V bias pulse to switch the charge state from Cs_T in (a) to another one, termed Cs_{H0}. The white grids in (a)–(c) represent the lattice of the Cu cations. Image conditions: $V_{bias} = 50$ mV and $I_t = 600$ pA. $\Delta\phi$ mappings of (d) Cs_T, (e) Cs_H and (f) Cs_{H0}. The black grids in (d)–(f) represent the lattice of the Cu cations. Solid circles in (d) and (e) indicate the locations of Cs_T and Cs_H, respectively. (g) XPS spectra of the Cs 3d peaks of pristine (black curve) and 0.8 ML Cs (red curve) covered ultrathin CuO films.

the LWF of the underlying substrate. A possible explanation is that the LWF changes induced by the cations and anions are not precisely on the ion sites, but rather deviate from the ion locations on the atomic scale, which is similar to the observations of the Au anion and K cation described above. Furthermore, similar to the case for the K_A species, the presence of Cs_T results in an obvious decrease in the LWF of the CuO substrate, covering an area of about 1.3 nm around Cs_T. Thus, the transferred charge of Cs_T is deduced to be about $0.73|e|$. A much larger charge transfer of Cs than K actually agrees with the fact that Cs possesses a much lower first ionization energy. At a coverage of 0.8 ML Cs on the CuO substrate (here one monolayer being defined as one Cs atom per CuO unit cell), the BE of Cs $3d_{5/2}$ is measured to be 725.0 eV in XPS, as shown in Fig. 3g, which is very close to that in Cs_2O, 725.1 eV, but much lower than that for metallic Cs, 726.3 eV, according to a report in the literature.[118] The XPS measurements substantiate that the Cs atoms are positively charged on the CuO substrate. It seems quite reasonable, but turns out to be very complicated when the LWF measurements are carried out. Fig. 3e shows that the apparent LWF decreases in an area of about 1.1 nm around the Cs_H cation on the CuO substrate. The transferred charge of Cs_T is deduced to be $0.52e$. Although both Cs_T and Cs_H are cationic according to the XPS measurements, the minimum of the apparent LWF caused by the Cs_H atom is lower by about 0.4 eV than that by the Cs_T atom, meaning that the charge transfer is site-dependent.

The charge state of Cs_T can be manipulated by the STM tip with an application of a sudden pulsed bias voltage. In Fig. 3c, the protrusion (Cs_T) turns into a rectangular depression (termed Cs_{H0}), which is randomly located on one of the four hollow sites fenced by four nearest Cu^{2+} cations, upon applying a bias voltage pulse of +5.0 V, on Cs_T. Similar tip manipulation on the Cs_H atom, however, leads to its desorption from the CuO substrate upon applying a bias voltage pulse of +4.0 V. These experimental facts indicate that the Cs_T and Cs_H atoms interact with the underlying CuO substrate to different extents.

Fig. 3f shows the $\Delta\phi$ mapping around Cs_{H0} after the tip manipulation on Cs_T as shown in Fig. 3a. The LWF slightly decreases at the locations of four Cu cations, as marked by the black dashed circles in Fig. 3f. The corresponding STM topographical image is given in Fig. 3c where the four Cu cations marked by the white solid circles become a little bit higher than those of the normal Cu cations previously snugged in the Cu–O chains and the four Cu cations marked by the white dashed circles cannot be topographically imaged. Compared to Cs_T and Cs_H, the influence of Cs_{H0} on the LWF of the monolayered CuO substrate is negligible, demonstrating that Cs_{H0} is essentially a neutral atom. The relocation and charge neutralization of Cs_T may possibly alter the geometric and electronic properties of its underlying CuO substrate, as deducted from the combined measurements of the STM image and the LWF variation mapping. However, a reverse voltage pulse applied on Cs_{H0} cannot trigger the opposite process from Cs_{H0} to Cs_T, indicating that the positive-to-neutral switch of the charge state is irreversible for the Cs_T species, unlike the case for the K_A species. The discrepancies between the charge states of individual Cs and K atoms on the monolayered CuO substrate actually reflect the difference in their intrinsic properties.

In contrast to the supported single Au atoms, experimentally both monodispersed K and Cs have no activity toward CO adsorption and oxidation. Due to their preferable donation nature of s-electrons and absence of valence d-electrons, alkali metals are usually employed as promotors rather than catalysts.

Interaction between supported Au and K atoms

Previous studies have suggested that the introduced Na or K cation can stabilize supported single Pt or Au atoms and further carry out water–gas shift reactions at low temperatures.[33–36] It's also suggested that the K–(OH) species formed by deposited K on hydroxylated TiO_2(110) are the active sites for Au clusters.[39] Therefore, the exploration of possible charge transfer between individual Au and alkali metal (K and Cs) atoms on an ultrathin CuO substrate should be of great interest in terms of the promoter effect of alkali elements on the activities of metallic ensembles in heterogeneous catalysis. To do this, Au and K are co-deposited onto a CuO substrate at RT and the LWFs around them are mapped. It's revealed that, at low coverage, most Au and K atoms remain monodispersed on the CuO monolayer as if they were deposited separately. For example, Fig. 4a shows the co-existence of three K single atoms and one K–Au pair, the latter being marked by the yellow square and its inter-atom separation being about 0.31 nm. The precise locations of the Au and K atoms in the K–Au pair are highlighted by the small and big circles, respectively. The apparent height of the paired K–Au is higher than that of an individual Au or K atom under the same scanning conditions, which suggests that an interaction between the K and Au atoms is established. Fig. 4b shows the corresponding $\Delta\phi$ mapping of the K–Au pair in Fig. 4a. The K–Au pair electronically interacts with its underlying CuO substrate within a region of about 1.9 nm in diameter, as marked by the dashed circle. To our surprise, the existing K atom (supposed to be positively charged) does not enhance the charge state of the nearby Au atom (supposed to be negatively charged), but rather they electronically cancel each other because the overall LWF of the K–Au pair in their core area in Fig. 4b approaches that of the bare CuO substrate. It looks like the positively charged K cation and negatively charged Au atom become electronically "neutralized" when they stick together. Meanwhile, the LWFs of the other three K atoms do not noticeably change with respect to that in Fig. 2c. Both experimental observations again imply that the charge transfer between the CuO substrate and K or Au is not long-range. The Au atom in the Au–K pair resembles its counterpart in a neutral state which is formed once one of its neighbouring lattice O atoms is removed by reaction with CO, as shown in Fig. 1. Therefore, the Au in the Au–K pair does indeed lose its activity towards CO oxidation, as confirmed by our experiments. When the Au stays far away from the K atoms, the LWFs around the Au and K atoms of the underlying CuO substrate do not interfere with each other, and the K atoms serve as an electronic spectator and hence do not influence the activity of the negatively charged Au atoms. It's deduced from our experiments that the interaction of Au with K in the K–Au pair weakens the Au–O interaction. This is similar to the situation where an Au single atom toward CO oxidation loses its activity once an O vacancy nearest to Au is created.

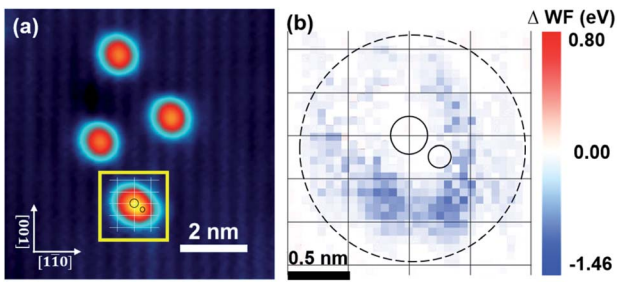

Fig. 4 (a) STM image of co-deposited Au and K atoms on the CuO monolayer. The crossing points of the white grid represent the Cu cations in the CuO lattice. Small and big circles indicate the Au and K atoms, respectively. (b) $\Delta\phi$ mapping of the region marked by the yellow square in (a). The crossing points of the black grid are the locations of the Cu cations. Small and big solid circles highlight the locations of the Au and K atoms, respectively. Image conditions: V_{bias} = 100 mV and I_t = 70 pA.

Bromine single atoms on Cu(111)

In contrast to alkali metals, halogens are another class of electronic additives serving as an electron acceptor. The charge transfer between halogen atoms and their underlying metal surfaces plays a crucial role in promoting the catalytic activity. Two methods have recently been explored in our group to prepare Br atoms on a surface. One is by decomposition of bromobenzene, which was evaporated onto a Cu(111) substrate and then annealed to about 500 K. The produced biphenyl molecules *via* the Ullmann coupling of the bromobenzene desorbed at this temperature and the remaining Br atoms assembled into islands with regular edges. The LWF around the Br island on the Cu substrate is increased by at least 1.5 eV, indicating significant electron transfer from the Cu(111) substrate to the Br atom.[120] The other is by AgBr electrolysis in an evaporator. In this method, Br atoms are directly deposited onto a substrate that is unnecessarily heated. Then, highly monodispersed Br atoms are achieved, as shown in Fig. 5a. The LWF around a single Br atom (Fig. 5b) on the Cu substrate is increased by about 0.8 eV (Fig. 5c), also confirming electron transfer from the Cu(111) substrate to the Br atom. These results are in great agreement with the conventional picture that halogen atoms typically withdraw electrons from the metal substrate, as measured by ultraviolet photoemission spectroscopy (UPS) or a Kelvin probe.[55,58–63,65] The transferred charge onto a Br atom deduced from the LWF mapping is about 0.19*e*. This shows again that the spatially resolved charge state of an additive provides more microscopic information that is not available from conventional surface techniques.

In fact, the microscopic picture of the charge transfer between the metal substrate and edge/internal Br atoms of the island is quite counterintuitive to the traditional one that the Br atoms at edges usually experience a more serious corrugation of electron density and hence cause a higher WF variation.[120] However, the traditional picture lacks the information that the electron density of the edge Br atoms can be smeared out by their contact with more neutral metal atoms in the substrate and the Smoluchowski smoothening effect.[121] This discrepancy between the macroscopic and microscopic pictures reminds that the charge transfer at

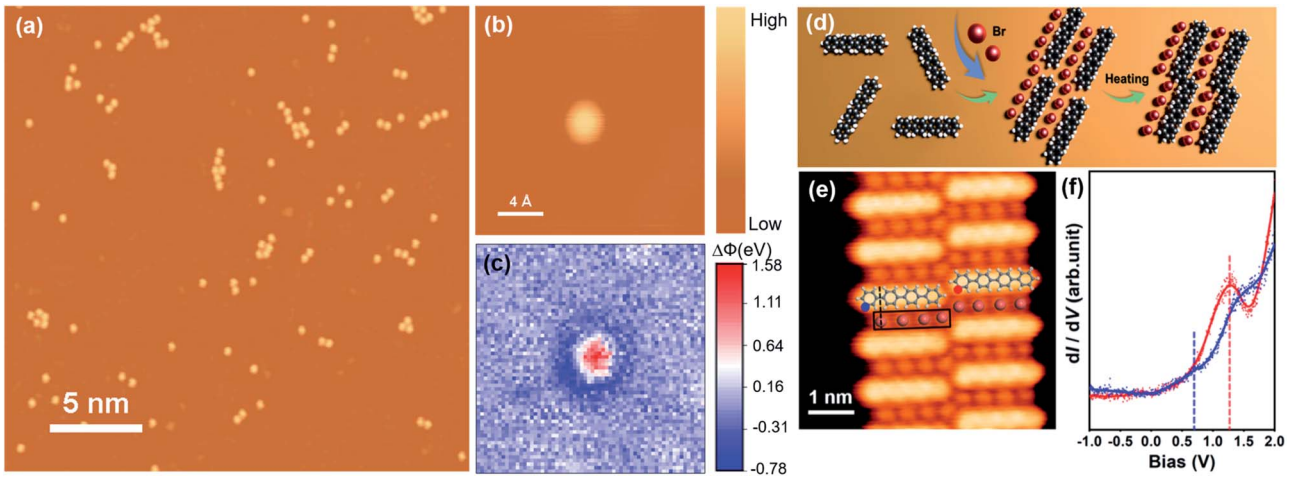

Fig. 5 (a) STM image of highly monodispersed Br atoms on Cu(111). (b) STM image of a single Br atom and (c) its corresponding $\Delta\phi$ mapping. (d) A schematic process of the coupling reaction mediated by the Br atoms. (e) High-resolution STM image of co-assembled Br atoms and Ph_4. (f) d*I*/d*V* spectra sampled at the sites highlighted by the coloured dots in (e). Reproduced with permission (d–f).[119] Copyright 2020, American Chemical Society.

a microscopic interface strongly depends on its locality, and hence the promoter effect on the catalytic performance in heterogeneous catalysis should be cautiously interpreted.

Lin *et al.*[119] reported that the introduced Br atoms on Cu(111) promoted the selectivity toward the coupling reaction of *p*-quaterphenyl (Ph_4) and *p*-quinquephenyl (Ph_5). The co-assembly of the Br atoms and Ph_4/Ph_5 with a specific ratio can efficiently increase their collision probability between two neighbouring Ph4 or Ph5 molecules (Fig. 5d). It is proven that the electronic structure of the reacting molecules can also be modified by the Br atoms nearby (Fig. 5e and f). Moreover, Liu *et al.*[122] have also proven that the Br atoms can promote the C–H bond activation of terminal alkynes on Ag(111) at room temperature.

Summary and prospects

Based on our recent studies and new data inputs, typical cases of charge transfer between single atoms and their supports on the atomic scale have been gathered in this perspective by stressing that a specific microscopic picture has to be established to understand the principles that govern the superb performance of SACs in various situations. It's widely appreciated that SACs possess the highest dispersion of and hence consume the least amount of precious metals. The exposed single metal atoms in SACs might be the most active due to their lowest coordination number on supports. Unfortunately, SACs are also thermally vulnerable because their single metal atoms can feasibly aggregate and cluster at elevated temperatures. Moreover, a single metal atom can form a strong interaction with its support so that the charge state and corresponding catalytic performance of the same single metal atom remarkably vary at different locations on the support. This is of particular importance in a nanosized SAC system where a single metal atom may be anchored to the corners, edges, kinks, steps, terraces and defects of the support. This may explain why many reported results of similar SACs are contradictory and even hard to reproduce in the literature.

Previously, people can only rely on density functional theory and other theories to estimate the charge state and electron transfer between a single atom and its support. But sophisticated theories have yet to be fully developed to treat locally charged systems, ionic oxides, non-conducting supports and ensembles of strong electronic interactions. On the other hand, conventional techniques in catalysis and surface science cannot experimentally provide microscopic information of the charge state and electron transfer in SACs. It becomes even more problematic in the cases where the metal atoms in later d and f blocks in the periodic table of elements may bilaterally donate and withdraw electrons from their supports.

To date, the only available techniques that can probe the local charge state and electron transfer in SACs are high-resolution spectroscopy techniques like STM and AFM. Only a limited number of model systems have been explored so far, and therefore a comprehensive database is still far from completion and people do not have a finger-pointing reference to understand the electronic properties of SACs. Nonetheless, scanning probe microscopy techniques turn out to be quite promising in principle to acquire local electronic information which is one of the most important aspects that dictate the catalytic performance of SACs.

Even with the limited amount of spatially resolved and quantitatively revealed information on the charge state and electron transfer of single atoms including Au, K and Cs on monolayered CuO as well as Br on Cu(111), one can immediately find that the situation becomes more complicated at the atomic level. The spatially resolved LWF variation caused by single atoms shows an obvious symmetry break which does not seem to be originating from the asymmetry of the STM tip, but instead from very local geometric and electronic corrugations that await further experimental and theoretical explorations. In addition, single-atom-induced variations of the LWFs at the

atomic level are not fully consistent with the simple picture, based on the information acquired by conventional XPS and UPS techniques, that the generated anions and cations increase and decrease the apparent WFs of the substrates, respectively. Yet, semi-quantitative or quantitative estimations of the charge transfer between single atoms and their underlying substrates could be deducted from the variations of the apparent LWFs.

In terms of the conventional promoter effect of alkali or halogen elements on the catalytic performance in heterogeneous catalysis, the described charge transfer between single Au and K atoms at a short distance on the CuO monolayer is so localized that they electronically cancel each other. This means that the charge transfer might take place directly in-between them or indirectly *via* the CuO substrate. Such a microscopic discovery suggests that the traditional explanation of alkali and halogen elements by electronic effects may fail on strongly ionic oxide or non-conducting supports in heterogeneous catalysis. Even on metallic substrates, the variations of the LWFs around the Br atoms in various spots within the Br islands are indicative that the extent of the charge transfer is very sensitive to the microscopic environment surrounding the concerned Br atom.

In summary, spatially resolved LWF measurements and quantitatively revealed electron transfer between single atoms and their underlying substrates do help us understand SACs at the atomic level. Single atoms may form strong interactions with the supports such that their catalytic performance becomes very sensitive to their specific locations on the supports. Therefore, a simple and general claim of the high efficiency of SACs could be misleading. This also applies to our understanding of the promoter effects of alkali and halogen elements in heterogeneous catalysis.

Conflicts of interest

There are no conflicts to declare.

Acknowledgements

This work was jointly supported by the NSFC (21821004, 21932001 and 21902174) and MOST (2017YFA0204702), China.

Notes and references

1 B. Qiao, A. Wang, X. Yang, L. F. Allard, Z. Jiang, Y. Cui, J. Liu, J. Li and T. Zhang, *Nat. Chem.*, 2011, **3**, 634–641.
2 X.-F. Yang, A. Wang, B. Qiao, J. Li, J. Liu and T. Zhang, *Acc. Chem. Res.*, 2013, **46**, 1740–1748.
3 B. Qiao, J.-X. Liang, A. Wang, C.-Q. Xu, J. Li, T. Zhang and J. J. Liu, *Nano Res.*, 2015, **8**, 2913–2924.
4 J. Lin, Y. Chen, Y. Zhou, L. Li, B. Qiao, A. Wang, J. Liu, X. Wang and T. Zhang, *AIChE J.*, 2017, **63**, 4003–4012.
5 R. Lang, W. Xi, J. C. Liu, Y. T. Cui, T. Li, A. F. Lee, F. Chen, Y. Chen, L. Li, L. Li, J. Lin, S. Miao, X. Liu, A. Q. Wang, X. Wang, J. Luo, B. Qiao, J. Li and T. Zhang, *Nat. Commun.*, 2019, **10**, 234.
6 A. Wang, J. Li and T. Zhang, *Nat. Rev. Chem.*, 2018, **2**, 65–81.
7 X. Li, X. Yang, Y. Huang, T. Zhang and B. Liu, *Adv. Mater.*, 2019, **31**, e1902031.
8 J. Zhou, Z. Xu, M. Xu, X. Zhou and K. Wu, *Nanoscale Adv.*, 2020, **2**, 3624–3631.
9 Z. Li, Y. Chen, S. Ji, Y. Tang, W. Chen, A. Li, J. Zhao, Y. Xiong, Y. Wu, Y. Gong, T. Yao, W. Liu, L. Zheng, J. Dong, Y. Wang, Z. Zhuang, W. Xing, C. T. He, C. Peng, W. C. Cheong, Q. Li, M. Zhang, Z. Chen, N. Fu, X. Gao, W. Zhu, J. Wan, J. Zhang, L. Gu, S. Wei, P. Hu, J. Luo, J. Li, C. Chen, Q. Peng, X. Duan, Y. Huang, X. M. Chen, D. Wang and Y. Li, *Nat. Chem.*, 2020, **12**, 764–772.
10 C. Chu, D. Huang, S. Gupta, S. Weon, J. Niu, E. Stavitski, C. Muhich and J. H. Kim, *Nat. Commun.*, 2021, **12**, 5179.
11 Z. Zhang, J. Liu, J. Wang, Q. Wang, Y. Wang, K. Wang, Z. Wang, M. Gu, Z. Tang, J. Lim, T. Zhao and F. Ciucci, *Nat. Commun.*, 2021, **12**, 5235.
12 X. Zhou, W. Yang, Q. Chen, Z. Geng, X. Shao, J. Li, Y. Wang, D. Dai, W. Chen, G. Xu, X. Yang and K. Wu, *J. Phys. Chem. C*, 2016, **120**, 1709–1715.
13 K. Ding, A. Gulec, A. M. Johnson, N. M. Schweitzer, G. D. Stucky, L. D. Marks and P. C. Stair, *Science*, 2015, **350**, 189–192.
14 Z. Zuo, S. Liu, Z. Wang, C. Liu, W. Huang, J. Huang and P. Liu, *ACS Catal.*, 2018, **8**, 9821–9835.
15 J. Wang, H. Tan, S. Yu and K. Zhou, *ACS Catal.*, 2015, **5**, 2873–2881.
16 A. Sanchez, S. Abbet, U. Heiz, W.-D. Schneider, H. Häkkinen, R. Barnett and U. Landman, *J. Phys. Chem. A*, 1999, **103**, 9573–9578.
17 B. Yoon, H. Häkkinen, U. Landman, A. S. Wörz, J.-M. Antonietti, S. Abbet, K. Judai and U. Heiz, *Science*, 2005, **307**, 403–407.
18 H. Tang, Y. Su, B. Zhang, A. F. Lee, M. A. Isaacs, K. Wilson, L. Li, Y. Ren, J. Huang, M. Haruta, B. Qiao, X. Liu, C. Jin, D. Su, J. Wang and T. Zhang, *Sci. Adv.*, 2017, **3**, e1700231.
19 W. D. Schneider, M. Heyde and H. J. Freund, *Chemistry*, 2018, **24**, 2317–2327.
20 I. X. Green, W. Tang, M. Neurock and J. T. Yates, *Science*, 2011, **333**, 736–739.
21 X. Zhang, H. Shi and B. Q. Xu, *Angew. Chem., Int. Ed.*, 2005, **44**, 7132–7135.
22 G. J. Hutchings, M. S. Hall, A. F. Carley, P. Landon, B. E. Solsona, C. J. Kiely, A. Herzing, M. Makkee, J. A. Moulijn, A. Overweg, J. C. Fierro-Gonzalez, J. Guzman and B. C. Gates, *J. Catal.*, 2006, **242**, 71–81.
23 M. F. Camellone and S. Fabris, *J. Am. Chem. Soc.*, 2009, **131**, 10473–10483.
24 D. Stolcic, M. Fischer, G. Gantefor, Y. D. Kim, Q. Sun and P. Jena, *J. Am. Chem. Soc.*, 2003, **125**, 2848–2849.
25 L. D. Socaciu, J. Hagen, T. M. Bernhardt, L. Woste, U. Heiz, H. Hakkinen and U. Landman, *J. Am. Chem. Soc.*, 2003, **125**, 10437–10445.
26 A. J. Therrien, A. J. R. Hensley, M. D. Marcinkowski, R. Zhang, F. R. Lucci, B. Coughlin, A. C. Schilling, J.-S. McEwen and E. C. H. Sykes, *Nat. Catal.*, 2018, **1**, 192–198.

27 X. Zhou, Q. Shen, K. Yuan, W. Yang, Q. Chen, Z. Geng, J. Zhang, X. Shao, W. Chen, G. Xu, X. Yang and K. Wu, *J. Am. Chem. Soc.*, 2018, **140**, 554–557.
28 A. J. Therrien, K. Groden, A. J. R. Hensley, A. C. Schilling, R. T. Hannagan, M. D. Marcinkowski, A. Pronschinske, F. R. Lucci, E. C. H. Sykes and J.-S. McEwen, *J. Catal.*, 2018, **364**, 166–173.
29 G. Ertl, *Angew. Chem., Int. Ed.*, 2008, **47**, 3524–3535.
30 O. Hinrichsen, F. Rosowski, M. Muhler and G. Ertl, *Chem. Eng. Sci.*, 1996, **51**, 1683–1690.
31 M. Muhler, F. Rosowski, O. Hinrichsen, A. Hornung and G. Ertl, in *Stud. Surf. Sci. Catal.*, Elsevier, 1996, vol. 101, pp. 317–326.
32 C. Zhang, F. Liu, Y. Zhai, H. Ariga, N. Yi, Y. Liu, K. Asakura, M. Flytzani-Stephanopoulos and H. He, *Angew. Chem., Int. Ed.*, 2012, **51**, 9628–9632.
33 Y. Zhai, D. Pierre, R. Si, W. Deng, P. Ferrin, A. U. Nilekar, G. Peng, J. A. Herron, D. C. Bell, H. Saltsburg, M. Mavrikakis and M. Flytzani-Stephanopoulos, *Science*, 2010, **329**, 1633–1636.
34 M. Yang, S. Li, Y. Wang, J. A. Herron, Y. Xu, L. F. Allard, S. Lee, J. Huang, M. Mavrikakis and M. Flytzani-Stephanopoulos, *Science*, 2014, **346**, 1498–1501.
35 B. Zugic, S. Zhang, D. C. Bell, F. F. Tao and M. Flytzani-Stephanopoulos, *J. Am. Chem. Soc.*, 2014, **136**, 3238–3245.
36 M. Yang, J. Liu, S. Lee, B. Zugic, J. Huang, L. F. Allard and M. Flytzani-Stephanopoulos, *J. Am. Chem. Soc.*, 2015, **137**, 3470–3473.
37 W. Ngantsoue-Hoc, Y. Zhang, R. J. O'Brien, M. Luo and B. H. Davis, *Appl. Catal., A*, 2002, **236**, 77–89.
38 A. B. Dongil, B. Bachiller-Baeza, E. Castillejos, N. Escalona, A. Guerrero-Ruiz and I. Rodríguez-Ramos, *Catal. Sci. Technol.*, 2016, **6**, 6118–6127.
39 D. C. Grinter, E. R. Remesal, S. Luo, J. Evans, S. D. Senanayake, D. J. Stacchiola, J. Graciani, J. F. Sanz and J. A. Rodriguez, *J. Phys. Chem. Lett.*, 2016, **7**, 3866–3872.
40 C. Park and M. A. Keane, *ChemPhysChem*, 2001, **2**, 733–741.
41 M. Vadekar and I. Pasternak, *Can. J. Chem. Eng.*, 1970, **48**, 216–218.
42 Y. Kiso, M. Tanaka, H. Nakamura, T. Yamasaki and K. Saeki, *J. Organomet. Chem.*, 1986, **312**, 357–364.
43 V. Choudhary and P. Jana, *J. Catal.*, 2007, **246**, 434–439.
44 S. T. Marshall and J. W. Medlin, *Surf. Sci. Rep.*, 2011, **66**, 173–184.
45 R. M. Lambert, R. L. Cropley, A. Husain and M. S. Tikhov, *Chem. Commun.*, 2003, 1184–1185, DOI: 10.1039/b302620e.
46 C. T. Campbell, *J. Catal.*, 1986, **99**, 28–38.
47 S. Y. Davydov and G. I. Sabirova, *Tech. Phys. Lett.*, 2011, **37**, 515–518.
48 S. Ahmad, P. Miró, M. Audiffred and T. Heine, *Solid State Commun.*, 2018, **272**, 22–27.
49 Z.-Y. Wang and D.-J. Shu, *J. Phys. Chem. C*, 2021, **125**, 19259–19267.
50 T. Aruga and Y. Murata, *Prog. Surf. Sci.*, 1989, **31**, 61–130.
51 H. P. Bonzel, *Surf. Sci. Rep.*, 1988, **8**, 43–125.
52 R. D. Diehl and R. McGrath, *Surf. Sci. Rep.*, 1996, **23**, 43–171.
53 H. Tochihara and S. Mizuno, *Prog. Surf. Sci.*, 1998, **58**, 1–74.
54 R. G. Jones, *Prog. Surf. Sci.*, 1988, **27**, 25–160.
55 W. Kai, W. Dezheng, D. Junzhuo, W. Xuming, C. Yuming, Z. Maosheng, Z. Runsheng and G. Xiexian, *Surf. Sci.*, 1992, **264**, 249–259.
56 K. Wu, D. Wang, X. Wei, Y. Cao and X. Guo, *J. Catal.*, 1993, **140**, 370–383.
57 K. Wu, D. Wang, X. Wei, Y. Cao and X. Guo, *Surf. Sci. Lett.*, 1993, **285**, L522–L524.
58 R. G. Jones and M. Kadodwala, *Surf. Sci.*, 1997, **370**, L219–L225.
59 P. Dowben and R. Jones, *Surf. Sci.*, 1979, **84**, 449–461.
60 P. Dowben and R. Jones, *Surf. Sci.*, 1979, **88**, 348–366.
61 E. Bertel, K. Schwaha and F. Netzer, *Surf. Sci.*, 1979, **83**, 439–452.
62 E. Bertel and F. Netzer, *Surf. Sci.*, 1980, **97**, 409–424.
63 S. K. Jo and J. White, *Surf. Sci.*, 1992, **261**, 111–117.
64 C. Jowett and B. Hopkins, *Surf. Sci.*, 1970, **22**, 392–410.
65 C. Benndorf and B. Krüger, *Surf. Sci.*, 1985, **151**, 271–288.
66 N. D. Lang, *Phys. Rev. B: Solid State*, 1971, **4**, 4234–4244.
67 Q. Zhu and S.-q. Wang, *J. Electrochem. Soc.*, 2016, **163**, H796–H808.
68 R. Lindsay, E. Michelangeli, B. G. Daniels, M. Polcik, A. Verdini, L. Floreano, A. Morgante, J. Muscat, N. M. Harrison and G. Thornton, *Surf. Sci.*, 2003, **547**, L859–L864.
69 U. Martinez, L. Giordano and G. Pacchioni, *J. Chem. Phys.*, 2008, **128**, 164707.
70 Z. Peng, B. Di, W. Li, D. Liu, X. Wen, H. Zhu, H. Song, Y. Zhang, C. Yin, X. Zhou and K. Wu, *Angew. Chem., Int. Ed.*, 2020, **59**, 14321–14325.
71 H. Chen, W. Rong, Z. Huang, Z. Peng, Z. Xu, J. Zhou, B. Di, X. Zhou and K. Wu, *J. Chem. Phys.*, 2019, **151**, 184703.
72 L. Olesen, M. Brandbyge, M. R. Sørensen, K. W. Jacobsen, E. Lægsgaard, I. Stensgaard and F. Besenbacher, *Phys. Rev. Lett.*, 1996, **76**, 1485.
73 L. Vitali, G. Levita, R. Ohmann, A. Comisso, A. De Vita and K. Kern, *Nat. Mater.*, 2010, **9**, 320–323.
74 F. Mohn, L. Gross, N. Moll and G. Meyer, *Nat. Nanotechnol.*, 2012, **7**, 227–231.
75 X. Wen, Y. Lin, Z. Huang, M. Diao, W. Zhao, J. Dai, L. Xing, H. Zhu, Z. Peng, D. Liu and K. Wu, *J. Phys. Chem. Lett.*, 2019, **10**, 6800–6806.
76 T. Konig, G. H. Simon, H.-P. Rust, G. Pacchioni, M. Heyde and H.-J. Freund, *J. Am. Chem. Soc.*, 2009, **131**, 17544–17545.
77 S. Schintke, S. Messerli, M. Pivetta, F. Patthey, L. Libioulle, M. Stengel, A. De Vita and W. D. Schneider, *Phys. Rev. Lett.*, 2001, **87**, 276801.
78 T. Yamada, J. Fujii and T. Mizoguchi, *Surf. Sci.*, 2001, **479**, 33–42.
79 J. Jia, K. Inoue, Y. Hasegawa, W. Yang and T. Sakurai, *Phys. Rev. B: Condens. Matter Mater. Phys.*, 1998, **58**, 1193.
80 T. Konig, G. H. Simon, H.-P. Rust and M. Heyde, *J. Phys. Chem. C*, 2009, **113**, 11301–11305.
81 Z. Huang, Z. Xu, J. Zhou, H. Chen, W. Rong, Y. Lin, X. Wen, H. Zhu and K. Wu, *J. Phys. Chem. C*, 2019, **123**, 17823–17828.
82 A. Sasahara, C. L. Pang and H. Onishi, *J. Phys. Chem. B*, 2006, **110**, 17584–17588.

83 L. Gross, F. Mohn, P. Liljeroth, J. Repp, F. J. Giessibl and G. Meyer, *Science*, 2009, **324**, 1428–1431.
84 Y. Zhang, O. Pluchery, L. Caillard, A. F. Lamic-Humblot, S. Casale, Y. J. Chabal and M. Salmeron, *Nano Lett.*, 2015, **15**, 51–55.
85 B. Mallada, A. Gallardo, M. Lamanec, B. de la Torre, V. Spirko, P. Hobza and P. Jelinek, *Science*, 2021, **374**, 863–867.
86 P. S. Bagus, V. Staemmler and C. Woll, *Phys. Rev. Lett.*, 2002, **89**, 096104.
87 A. Michaelides, P. Hu, M. H. Lee, A. Alavi and D. A. King, *Phys. Rev. Lett.*, 2003, **90**, 246103.
88 T. C. Leung, C. L. Kao, W. S. Su, Y. J. Feng and C. T. Chan, *Phys. Rev. B: Condens. Matter Mater. Phys.*, 2003, **68**, 195408.
89 F. Albrecht, M. Fleischmann, M. Scheer, L. Gross and J. Repp, *Phys. Rev. B: Condens. Matter Mater. Phys.*, 2015, **92**, 235443.
90 N. D. Lang, *Phys. Rev. B: Condens. Matter Mater. Phys.*, 1988, **37**, 10395–10398.
91 T. Aoki and T. Yokoyama, *Phys. Rev. B: Condens. Matter Mater. Phys.*, 2014, **89**, 155423.
92 M. Becker and R. Berndt, *Phys. Rev. B: Condens. Matter Mater. Phys.*, 2010, **81**, 035426.
93 H. Geistlinger, *Sens. Actuators, B*, 1993, **17**, 47–60.
94 H. Schwarz, *Catal. Sci. Technol.*, 2017, **7**, 4302–4314.
95 C. Zhu, S. Fu, Q. Shi, D. Du and Y. Lin, *Angew. Chem., Int. Ed.*, 2017, **56**, 13944–13960.
96 H. Zhang, G. Liu, L. Shi and J. Ye, *Adv. Energy Mater.*, 2018, **8**, 1701343.
97 G. Giannakakis, M. Flytzani-Stephanopoulos and E. C. H. Sykes, *Acc. Chem. Res.*, 2018, **52**, 237–247.
98 M. T. Darby, M. Stamatakis, A. Michaelides and E. C. H. Sykes, *J. Phys. Chem. Lett.*, 2018, **9**, 5636–5646.
99 X. Cui, W. Li, P. Ryabchuk, K. Junge and M. Beller, *Nat. Catal.*, 2018, **1**, 385–397.
100 S. Liang, C. Hao and Y. Shi, *ChemCatChem*, 2015, **7**, 2559–2567.
101 J. Liu, *ACS Catal.*, 2017, **7**, 34–59.
102 Z. Li, D. Wang, Y. Wu and Y. Li, *Natl. Sci. Rev.*, 2018, **5**, 673–689.
103 Y. Chen, S. Ji, C. Chen, Q. Peng, D. Wang and Y. Li, *Joule*, 2018, **2**, 1242–1264.
104 M. J. Hülsey, J. Zhang and N. Yan, *Adv. Mater.*, 2018, **30**, 1802304.
105 L. Liu and A. Corma, *Chem. Rev.*, 2018, **118**, 4981–5079.
106 Y. Wang, J. Mao, X. Meng, L. Yu, D. Deng and X. Bao, *Chem. Rev.*, 2018, **119**, 1806–1854.
107 Y. Guo, R. Lang and B. Qiao, *Catalysts*, 2019, **9**, 135.
108 G. S. Parkinson, *Catal. Lett.*, 2019, **149**, 1137–1146.
109 Z. Chen, L. Chen, C. Yang and Q. Jiang, *J. Mater. Chem. A*, 2019, **7**, 3492–3515.
110 D. Liu, Q. He, S. Ding and L. Song, *Adv. Energy Mater.*, 2020, **10**, 2001482.
111 J. C. Liu, Y. G. Wang and J. Li, *J. Am. Chem. Soc.*, 2017, **139**, 6190–6199.
112 D. J. Coulman, J. Wintterlin, R. J. Behm and G. Ertl, *Phys. Rev. Lett.*, 1990, **64**, 1761–1764.
113 F. Jensen, F. Besenbacher, E. Laegsgaard and I. Stensgaard, *Phys. Rev. B: Condens. Matter Mater. Phys.*, 1990, **41**, 10233–10236.
114 K. Kern, H. Niehus, A. Schatz, P. Zeppenfeld, J. Goerge and G. Comsa, *Phys. Rev. Lett.*, 1991, **67**, 855–858.
115 V. Pouthier, C. Ramseyer, C. Girardet, P. Zeppenfeld, V. Diercks and R. Halmer, *Phys. Rev. B: Condens. Matter Mater. Phys.*, 1998, **58**, 9998.
116 L. Ruan, F. Besenbacher, I. I. Stensgaard and E. Laegsgaard, *Phys. Rev. Lett.*, 1993, **70**, 4079–4082.
117 A. Yurtsever, Y. Sugimoto, M. Abe, K. Matsunaga, I. Tanaka and S. Morita, *Phys. Rev. B: Condens. Matter Mater. Phys.*, 2011, **84**, 085413.
118 G. Ebbinghaus and A. Simon, *Chem. Phys.*, 1979, **43**, 117–133.
119 Y. Lin, Z. Huang, X. Wen, W. Rong, Z. Peng, M. Diao, L. Xing, J. Dai, X. Zhou and K. Wu, *ACS Nano*, 2020, **14**, 17134–17141.
120 Z. Huang, Y. Lin, C. Han, Y.-Y. Sun, K. Wu and W. Chen, *J. Phys. Chem. C*, 2021, **125**, 7944–7949.
121 R. Smoluchowski, *Phys. Rev.*, 1941, **60**, 661–674.
122 J. Liu, Q. Chen, Q. He, Y. Zhang, X. Fu, Y. Wang, D. Zhao, W. Chen, G. Q. Xu and K. Wu, *Phys. Chem. Chem. Phys.*, 2018, **20**, 11081–11088.